R&D for a Detector at the International Linear Collider

W. Lohmann
DESY, D-15738 Zeuthen, Germany

Research and development programs for a detector at the ILC started in Asia, North America and Europe several years ago. A survey is given on ongoing activities and on recent results obtained for all sub-detectors.

1. INTRODUCTION

In the past detector research and development was done in the three regions, Asia, Europe and North America, closely connected to the linear collider projects pursued in the corresponding region. Since the technology choice was made in August 2004, the impact of the accelerator parameters, in particular the time structure of the bunch trains, are now the same for all regions. Hence a chance is given to collaborate more closely in the future, to tackle many open questions in a collaborative spirit and to structure more efficiently the world-wide effort. Here an overview is given on the detector R&D efforts and on recent results from all three regions.

An example for a linear collider detector, the "Global Large Detector" is given in Figure 1. Other options, denoted as LDC and SDC [1] have in general the same structure. Around the interaction region (IP) the following sub-detectors are planned: a vertex detector, a central tracker, an electromagnetic calorimeter, a hadron calorimeter and a muon detector. All sub-detectors, apart the muon detectors, are placed inside a solenoid magnet, which induces a magnetic field between 3 and 5 Tesla, depending on the detector concept. At small polar angles the tracking

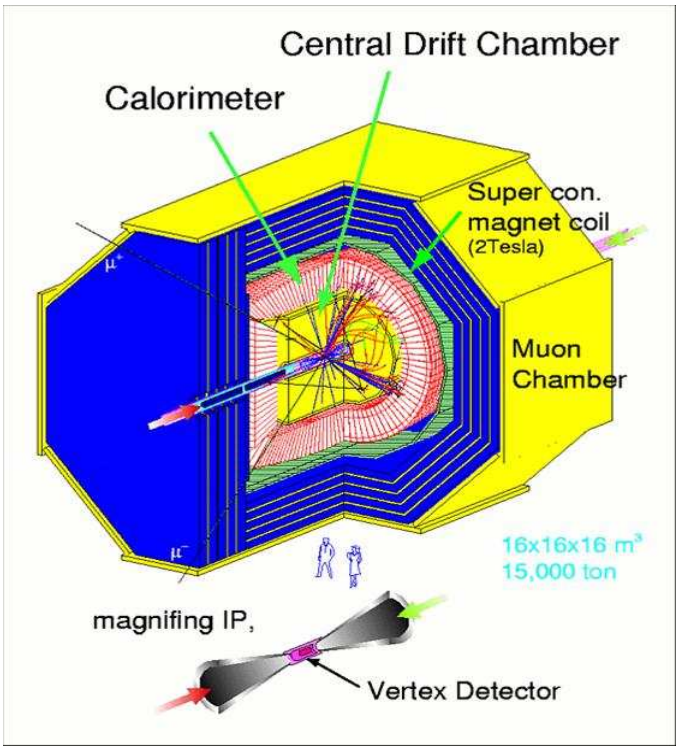

Figure 1: A detector proposed for the ILC, the GLD concept, chosen as an example.

performance is improved by 'forward tracking' devices. At very small polar angles special calorimeters are planned to measure precisely the luminosity and to reach good hermeticity of the detector. I'll give an overview on the R&D for each of these sub-detectors.

2. REQUIREMENTS FROM PHYSICS

One of the most challenging topics of the physics program is to explore the electroweak symmetry breaking. In the Standard Model particles acquire mass via the Higgs mechanism, resulting in a scalar particle of unknown mass, the Higgs boson. A detector at a linear collider has to be designed to explore the profile of the Higgs boson. If no Higgs boson exists, gauge bosons will strongly interact at high energy. To measure this effect pair produced W bosons in association with neutrinos must be identified and analysed. More complex Higgs sectors are predicted by super-symmetry. If super-symmetry exists, a detector at a linear collider must be able to explore the structure of the Higgs boson sector and to measure the spectrum and couplings of super-symmetric particles. Detailed Monte Carlo simulations for these scenarios and for many other extensions of the Standard Model have been done to derive benchmarks for the performance of the sub-detectors. Comparing these requirements with the performance reached at detectors operated in previous or currently running experiments at e^+e^- or $e^{\pm}p$ colliders, the following conclusions can be drawn:

- The ability of the vertex detector to detect secondary vertices, expressed as impact parameter resolution, must be about 10 times better than at LEP detectors and 3 times better than at the SLD detector.
- The momentum resolution of the tracker must be 10 times better than at LEP detectors.
- The jet energy measurement must be 3 times better than at LEP or HERA detectors.
- The luminosity measurement must be 3 times better than at LEP.

For new particle searches hermeticity is essential, requiring calorimetry down to polar angles of about 5 mrad.

3. LUMINOSITY MEASUREMENT AND INSTRUMENTATION OF THE VERY FORWARD REGION

A possible layout of the very forward region of the ILC detector[1] is shown in Figure 2. The BeamCal adjacent to the beam-pipe covers a polar angle range between 4 and 28 mrad. It is strongly affected by electrons and positrons originating from beamstrahlung photon conversions. As an example, a simulation of the energy density per bunch crossing at the front face of the BeamCal is shown in Figure 3. The energy density distribution depends on the beam parameters and will be measured for a fast beam tuning to ensure maximum luminosity. The total dose expected for one year of running amounts up to to 10 MGy for sensors near the beam-pipe. Hence radiation hard sensors must be used. In addition, high-energy electrons from the two-photon process have to be measured or at least vetoed to angles as close as possible to the beam. Fine granularity is necessary to identify the localised depositions from high energy electrons on top of the broader spread of energy from beamstrahlung remnants. Monte Carlo studies favor a compact silicon or diamond tungsten sandwich calorimeter with a Moliere radius of about one cm [3]. The requirements on the sensors are very good linearity over a dynamic range of at least 1000, very good homogeneity, fast response and stable operation under high electromagnetic doses. First results of studies with CVD diamond sensors are promising.

[1] This layout is designed for head-on collisons or a small crossing angle. For 20 mrad crossing angle it must be reconsidered.

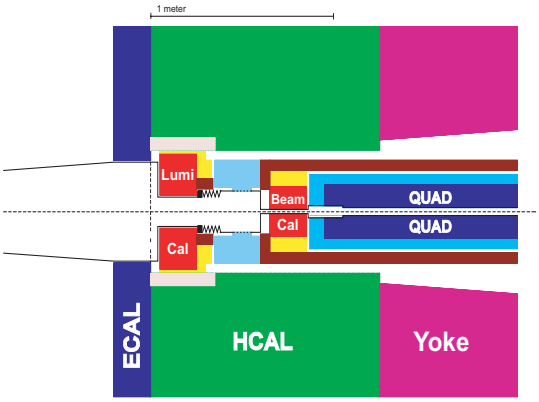

Figure 2: The forward calorimeters BeamCal and LumiCal. The conical beam-pipe on the left points to the interaction region. The distance between the interaction point and the LumiCal is about 3 m. ECAL and HCAL are the electromagnetic and hadron calorimeters, respectively, and QUAD is the last quadrupole of the beam delivery system.

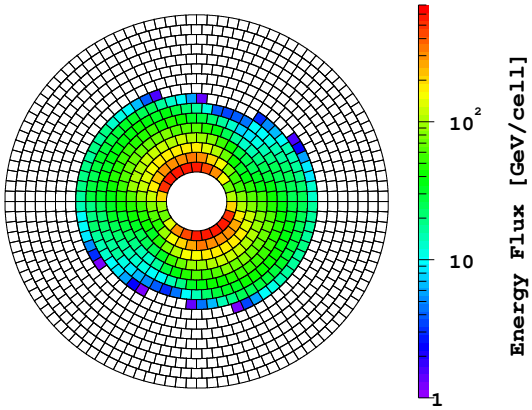

Figure 3: Energy density of beamstrahlung remnants per bunch crossing in the R-ϕ plane at the face of the BeamCal. The centre-of-mass energy is 500 GeV and TESLA machine parameter settings are used [2].

The LumiCal is the luminometer of the detector. The goal is to measure the luminosity with an accuracy better than 10^{-3}. We simulate a silicon tungsten calorimeter to estimate the requirements on the sensor segmentation and on the tolerances of the mechanical frame and its position [3]. The shower reconstruction algorithm is optimised to keep the bias on the polar angle measurement minimal. In future the effort will be extended to sensor studies and the design of a mechanical frame.

4. RECONSTRUCTION OF SECONDARY VERTICES

The detection of secondary vertices allows to identify b- and c-quark jets and tau leptons. In addition, the measurement of the jet charge-sign improves significantly the physics potential of the detector [4]. The performance goal for a vertex detector is expressed as the impact parameter resolution in the (rϕ) and (rz) planes,

$$\sigma_{r\phi} = \sigma_{rz} = 3.8 \oplus 7.8/(p \cdot sin^{3/2}\theta)\mu\text{m},$$

where p is the momentum of the particle and θ the polar angle. It can be reached with silicon pixel sensors with a pitch of about 20μm, five detector layers with a thickness of less than 0.1 X_0 per layer, a radius of the beam-pipe of less than 1.5 cm and a thin-walled beam-pipe. The occupancy expected for the operation of the detector under realistic conditions requires a readout every 50 μs during the bunch train of the ILC. A layout prepared for the TESLA detector [2] is shown in Figure 4. The vertex detector may suffer by electromagnetic pickup from the wake-fields of the bunches (EMI) [5]. Several technologies for the pixel sensors are under investigation. I describe, as examples, the DEPFET (DEPleted Field Effect Transistor) [6], the CCD (Charged Coupled Devices) [7] and the MAPS (Monolithic Active Pixel Sensors) [8] technologies[2]. DEPFET is a relatively new technology for the ILC.

[2]There are activities in many other fields like CAP-Continuously Active Pixel, HAPS-Hybrid Active Pixel, SoI- Silicon on Insulator, which are interesting as well.

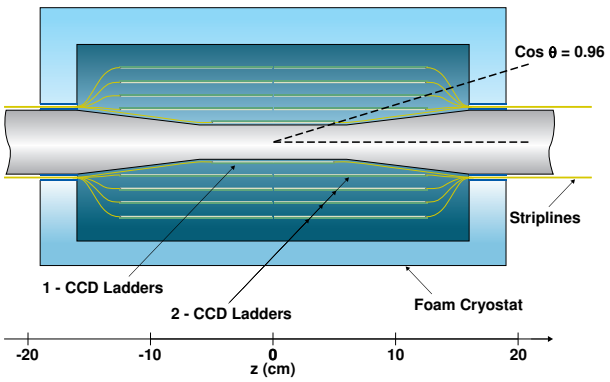

Figure 4: A possible layout of the vertex detector. Five layers of thin silicon pixel detectors surround the interaction region. In this particular case the CCD technology is chosen, requiring a foam made cryostat to keep the temperature at 200^0 K.

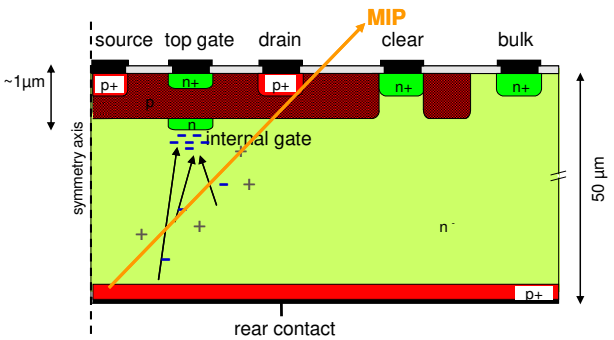

Figure 5: The structure of a DEPFET pixel. Electrons liberated by a charged particle crossing are collected at the internal gate which controls the current in the FET transistor. After the read out, a clear pulse removes the electrons from the gate, making the pixel sensitive for the next particle.

CCDs and MAPS developments are already advanced.

4.1. DEPFET

A DEPFET pixel sensor consists of a fully depleted silicon substrate with an integrated field effect transistor on top of each pixel. The structure of a pixel is shown in Figure 5. The potential between the top side and rear end of the pixel has a minimum below the transistor. Electrons created by ionisation in the depleted substrate drift to the potential minimum, serving as an internal gate and are trapped there. The charge collected on the internal gate controls the current in the transistor. Hence the signal is amplified resulting in a signal-to-noise ratio of 40 at room temperature. After the readout the signal charge has to be cleared. Since only the row which is actually read out is powered, a very low net power consumption is achieved. For a full five layer detector 4 W is estimated. It was proved in the laboratory that sensors can be thinned down to 50 μm, reaching the goal of 0.1 X_0 per layer. A prototype of a 64x128 pixel matrix with 10x30 μm pixel size was recently operated in a test-beam. Prototypes of the readout and switcher ICs are developed. A readout frequency of 25 MHz and a fast clear within 10 ns was reached with tolerable noise. The radiation hardness of the pixel sensors was tested with a ^{60}Co source up to 1 Mrad, sufficient for the operation in the ILC detector for 5 years. The next steps will be the design of a larger pixel matrix, the redesign of the switcher and readout chips approaching 50 MHz necessary at ILC, and the test of the radiation hardness of the full system.

4.2. CCD and MAPS

In these technologies the charge is collected from a partly depleted epitaxial layer of 10-20 μm thickness. CCDs were used successfully at the SLD detector [9]. The major challenges are the readout speed, thin sensors and radiation hardness. A special readout chip is developed for column parallel readout containing a preamplifier, a 5-bit ADC per column and a FIFO memory. The readout frequency of the current device is 25 MHz. A new version designed for 50 MHz, containing also sparse readout circuitry, is in the test phase. A test of a full detector module is foreseen in 2010.

The use of In-situ Storage Image Sensors (ISIS) allows to store the signals on the pixel for readout until the bunch train has passed. This technique promises robustness against EMI. As an example, a circular memory is shown in

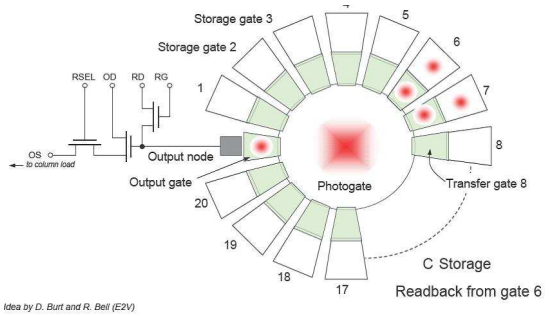

Figure 6: The layout of a circular ISIS memory. 20 independent storage gates are around the central photo-gate. Charge collected on the photo-gate is transfered to the storage gates during the bunch train and read out after the bunch train has passed.

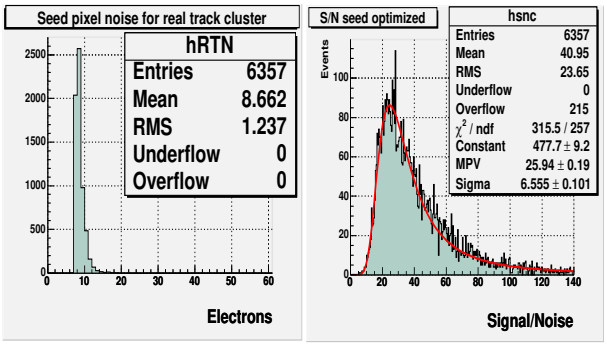

Figure 7: The distribution of the pixel noise and the S/N from a test-beam measurement using 120 GeV pions at CERN.

Figure 6. Another solution to be immune against EMI is to use smaller pixels, e.g. 5 x 5 μm^2 (Fine Pixel CCD, FPCCD) [10] and readout between the trains. For both technologies also the readout speed can be reduced.

In the case of MAPS a preamplifier is integrated on each pixel. The rows of sensing transistors are successively switched on by gating lines. The signal is then transported to the edge of the active area by means of readout lines. Prototype sensors are produced with, e. g. 20 x 20 μm^2 pixel size, and tested in a beam. The distribution of the noise and S/N ratio is shown in Figure 7. The most probable value of the S/N is about 25, the efficiency larger than 99% and the spatial resolution about 1.5 μm. Irradiation with electrons up to several 100 kRad and neutrons fluxes of 10^{12} neutrons cm^{-2} result in a slight reduction of the S/N ratio but no loss in efficiency. MAPS sensors are thinned down to the epitaxial layer and operated with reasonable S/N ratio. Also the integration of the signal charge storage capacitors to be read out in between the trains is under development.

Mechanical studies for a proper support structure are ongoing for all technologies. Materials like silicon carbide foam or CVD diamonds are considered for a stiff mechanical frame.

5. CENTRAL TRACKER

Two designs for a central tracker are pursued. One is based on a gaseous detector operated as Time Projection Chamber (TPC), the other relies on concentric cylinders equipped with silicon strip sensors. Monte Carlo estimates have shown that a momentum resolution of about $\sigma(1/p) = 6 \cdot 10^{-5}$ GeV^{-1} can be matched by both technologies.

5.1. TPC

TPCs were used successfully in the LEP experiments ALEPH [11] and DELPHI [12]. The R&D is focused on the improvement of the momentum resolution by novel gas amplification techniques, delivering also more hits along a track, novel gas mixtures and a field cage allowing to maintain an extremely homogeneous electric field up to the edges of the device [13]. In addition, the performance of the TPC in a large solenoidal magnetic field must be understood. The performance goals are a point resolution of 100 μm in the (R,ϕ) plane, 500 μm in z and double track resolutions of about 2 mm and 5 mm in the (R,ϕ) and z coordinates, respectively. Several small TPC prototypes are operated in many labs to approach these goals. The gas amplification is obtained using, like in the past, wires, or novel technologies. These are one or more layers of Gas Electron Multipliers (GEM) foils or Micromegas. Measurements are done with cosmics and test-beams. As an example in Figure 8 (left) the resolution in x (corresponding to R,ϕ) is shown as a function of the drift distance for magnetic fields between one and 4 Tesla. A difference is still seen between the measured resolution in (R,ϕ) and the expectation from simulations, which needs more detailed studies

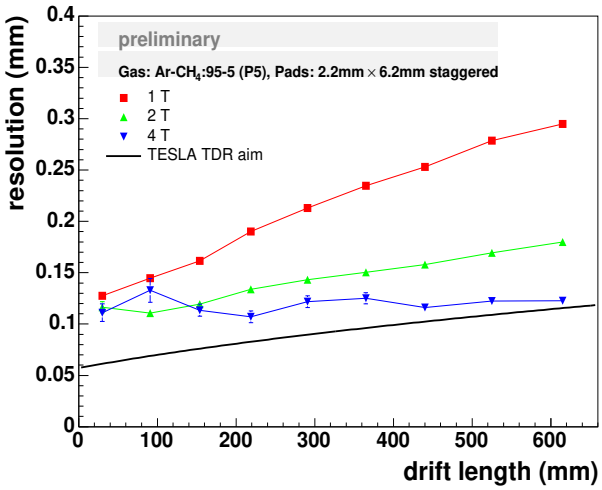

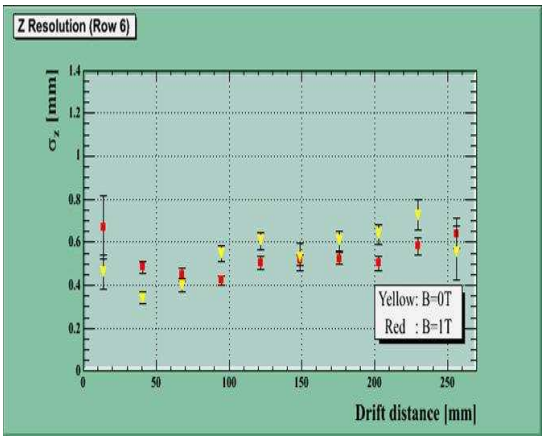

Figure 8: The resolutions of prototype TPCs. Left is shown the resolution in x (R,ϕ) as a function of the drift distance for different magnetic fields B measured with cosmics. Right is shown the resolution in z as a function of the drift distance from test-beam data for zero B-field and B = 1T.

in future. Also shown on the right is the resolution is z as a function of the drift distance measured in a test-beam at KEK. Here the goal is nearly reached. A measurement of the energy loss, dE/dx, for protons and pions of one GeV is shown in Figure 9. Protons and pions are clearly separated, demonstrating the potential of a TPC for particle

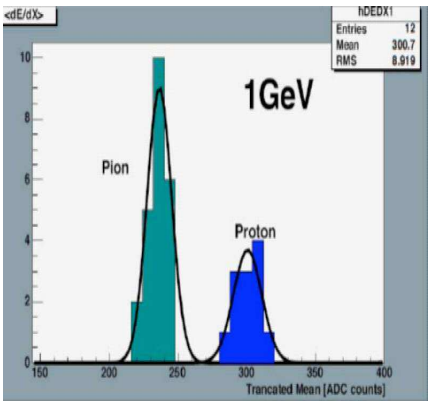

Figure 9: dE/dx measured for 1 GeV protons and pions using the KEK test-beam.

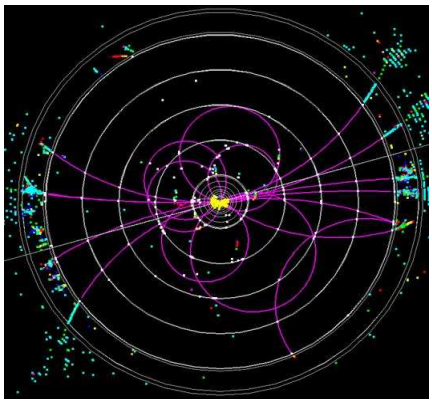

Figure 10: An electron positron annihilation event as seen by a full silicon tracker consisting of 5 concentric cylinders equipped with silicon strip detectors.

identification.

The measurements at the test-beam at KEK are going on using different gas amplification schemes, giving the opportunity to compare the performance using the same TPC frame. So far GEMs and Micromegas show similar operation stability and resolutions.

The next step will be the construction of a larger prototype. The goal is a detailed understanding of the different gas amplification techniques, to get experience in the manufacturing of the end-plates and the field-cage and to test readout electronics. First test measurements are planned at the end of 2006.

5.2. Silicon Tracker SiD

The track reconstruction will be performed using hits from silicon strip detectors placed on concentric cylinders around the beam-pipe. A simulated e^+e^- annihilation event is shown in Figure 10.

A space point resolution of about 5 μm can be reached [3] resulting in a momentum resolution similar to the TPC but in a smaller tracker radius and a magnetic field of 5 T.

The outermost cylinder is about 3.4 m long. To instrument it with silicon strip modules two concepts are followed. In the first [14] long half-ladders up to 1.7 m length consist of daisy-chained silicon sensors, resulting in large strip capacitances. The R&D is focused to the development of low noise preamplifiers with shaping times of several μs [15]. A first prototype of a readout chip, shown in Figure 11 [16], containing 16 channels, is under test. Test-beam

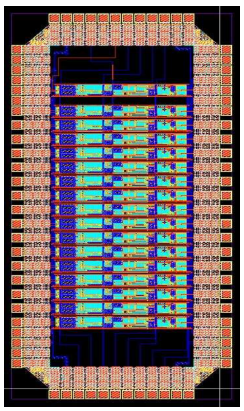

Figure 11: A 16 channel FE chip optimised for the readout of long silicon strips, containing preamplifier, shaper and ADC. The length of the chip is 3 mm.

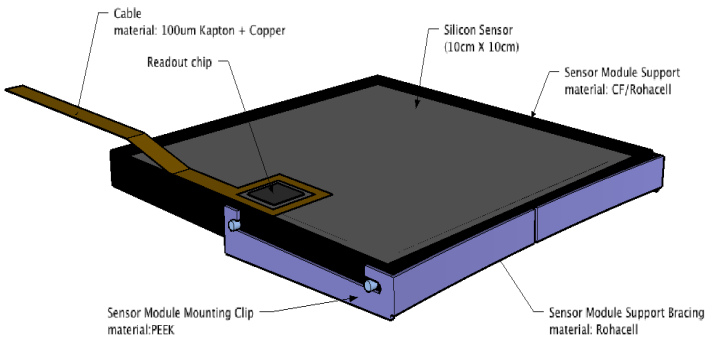

Figure 12: A silicon strip sensor module as proposed for the SiD detector. All sensors of the 10x10 cm^2 module are connected to one readout chip.

measurements with long ladders are planned at the fall of 2006. Issues are measurements of S/N, the efficiency and the resolution as a function of the incident angle.

The second concept[17] foresees quadratic sensor modules, as shown in Figure 12, to avoid large sensor capacitances. The whole module will be read out by one FE chip which is in the design stage.

The support cylinders will be built as carbon fibre structures with rohacell elements for sensor positioning, keeping the material per cylinder below 1% X_0. R&D for the mechanics design is ongoing [18].

5.3. Forward Tracking

Using only the barrel part of the detector the tracking performance deteriorates for polar angles below 30^0. Hence, additional tracking devices must be installed in the forward direction. For the SiD the cylinders are supplemented with disks carrying silicon strip or pad detectors. In the case of a TPC the forward region will be instrumented with additional silicon disks. A possible design of the forward tracking [14] is shown in Figure 13. Several disks instrumented with silicon pixel and strip sensors ensure a very good track measurements also at small polar angles. In addition, between the TPC end-plates and the ECAL drift tubes are foreseen. Simulations are done with silicon sensors and straw tubes in front of the TPC end-plates [19], showing that a good tracking performance can be maintained for polar angles down to 7^0. Also GEM chambers are proposed for the instrumentation of the polar angle region down to the mask [20]. Prototypes of chambers with an area of 10x10 cm^2 are studied with cosmics.

[3] For a readout pitch is 50 μm

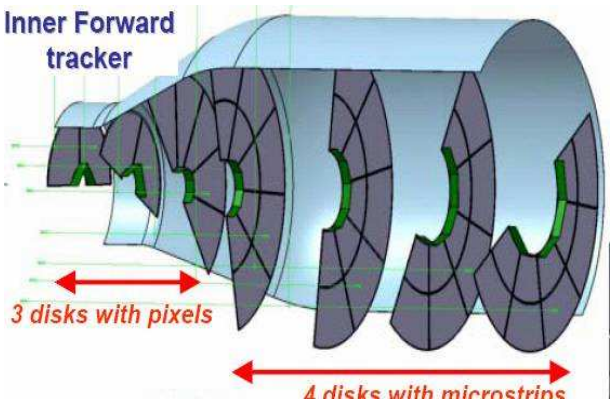

Figure 13: The instrumentation of the forward region as proposed in the SiLC project [14]. Several disks equipped with pixel and silicon strip sensors are foreseen.

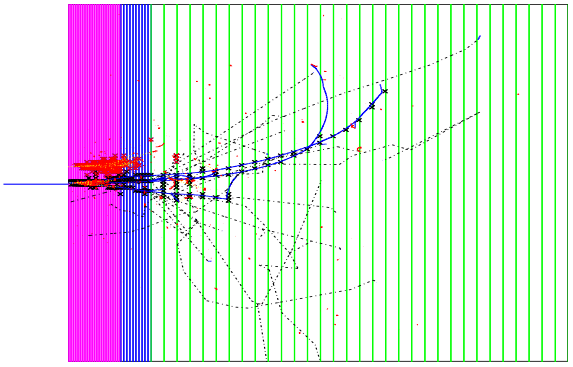

Figure 14: The showers of a charged hadron and a photon in fine segmented electromagnetic and hadron calorimeters. The distance between the impact points of the two particles onto the electromagnetic calorimeter is 5 cm. (by courtesy of A. Raspereza)

6. CALORIMETRY

The jet energy resolution goal of $\sigma_E/E = 30\%/\sqrt{E}$ can be reached with the particle flow concept. If a track is matched to local energy depositions (clusters) in the calorimeters, the track measurement is used to determine the four-momentum of the particle. Clusters without a matched track are regarded as neutral clusters and their energy and direction is determined from the deposition in the calorimeter. To realize this concept compact and fine segmented electromagnetic and hadron calorimeters are needed. In addition, minimum ionising particles, mips, must be detected. For certain new particle searches it is necessary to determine the direction of electromagnetic showers solely from the depositions in the calorimeter. As an example the showers of a charged hadron, associated to a track, and of a nearby photon is shown in Figure 14. The two showers are clearly separated and can be treated as individual particles.

6.1. Electromagnetic Calorimeters

Under study are silicon-tungsten and scintillator-tungsten sandwich calorimeters. Pure silicon-tungsten calorimeters are relatively expensive. For a very large detector the scintillator-tungsten option seems to be more appropriate. Also hybrid structures, where silicon is partly replaced by scintillators, are investigated.

6.1.1. Silicon Tungsten Calorimetry

The possible structure of a silicon tungsten sandwich calorimeter, as proposed by the CALICE collaboration [21] is shown in Figure 15. The thickness of the absorber layers is 0.4 X_0 for the first 12 radiation lengths in depth and 1.2 X_0 for the adjacent 12 radiation lengths. The Moliere radius is a bit larger than the pad size.

Two groups have constructed prototype calorimeters which are operated in test-beams. The calorimeters are instrumented with silicon sensors with pads of about 1x1 cm^2 size. An assembled prototype sensor is shown in Figure 16. The numbers of fully equipped readout channels are about 3000 [22] and 650 [23], respectively. As a preliminary result, the integrated signal for electrons of 1, 2 and 3 GeV is shown in Figure 17 [22]. Also dedicated FE electronics is under development and will be improved [24]. Both groups will continue the test-beam measurement with completed or upgraded prototype calorimeters soon.

A different sensor structure is shown in Figure 18 [25]. Tests of the first prototype sensors are very promising. A special readout chip is under development placed directly on the sensor and reading out all 1024 pixels [26].

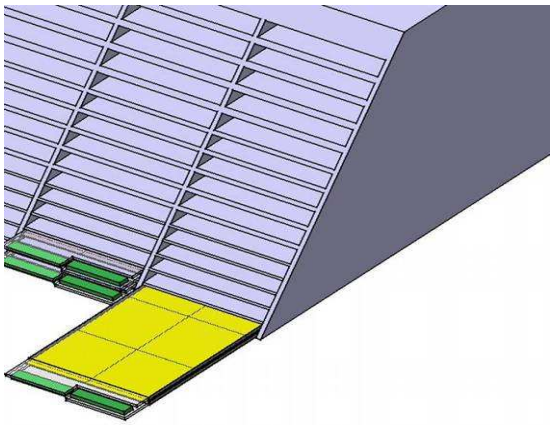

Figure 15: The structure of the silicon tungsten calorimeter, as proposed by the CALICE collaboration. The slots in the tungsten frame are equipped with silicon sensor planes. The sensors are structured into pads of about 1x1 cm^2 size.

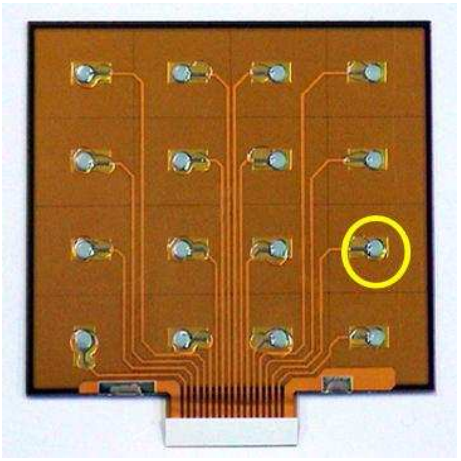

Figure 16: An assembled silicon pad sensor for the prototype electromagnetic calorimeter tested at in the beam

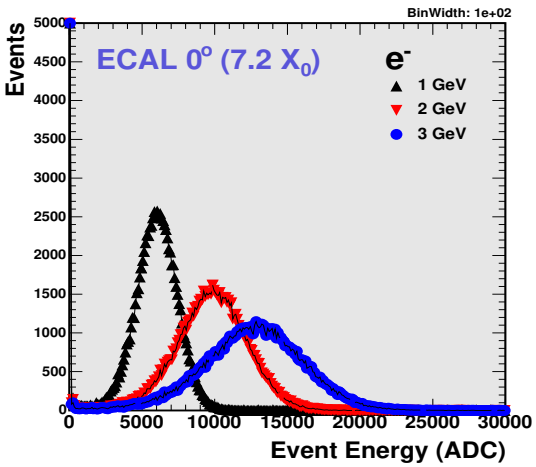

Figure 17: The energy response for electrons of 1, 2 and 3 GeV in the CALICE prototype calorimeter.

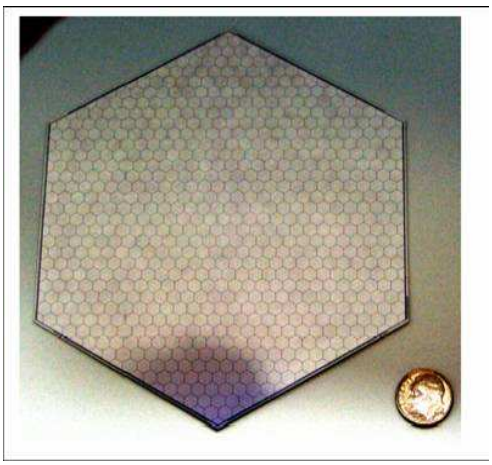

Figure 18: A silicon sensor prototype with hexagon pads.

6.1.2. Silicon-Scintillator Lead Sandwich Calorimeter

A prototype of a sandwich calorimeter consisting of 45 scintillator planes and three planes of silicon pads interspersed between lead absorber disks [27] was built and operated in a test-beam. As an example, the measured energy resolution, parametrised as $11\%/\sqrt{E}$, is shown in Figure 19.

6.1.3. Scintillator Sandwich Calorimeter

For a calorimeter with a large radius a fine segmented scintillator based sandwich calorimeter may have a particle flow performance similar to a compact silicon-tungsten calorimeter but will be of lower costs. A prototype using lead as absorber and scintillator strips with wavelength shifting fibers read out by multichannel photo-multipliers is shown in Figure 20 [28]. The measured energy resolution is similar to the silicon-scintillator calorimeter. Currently novel Geiger mode photo-diodes, called silicon photo-multipliers, SiPMs, are investigated in detail. In case the results are satisfactory, the multichannel photo-multipliers will be replaced by SiPMs. A prototype optimised for particle flow measurement will be ready for beam test at the end of 2007.

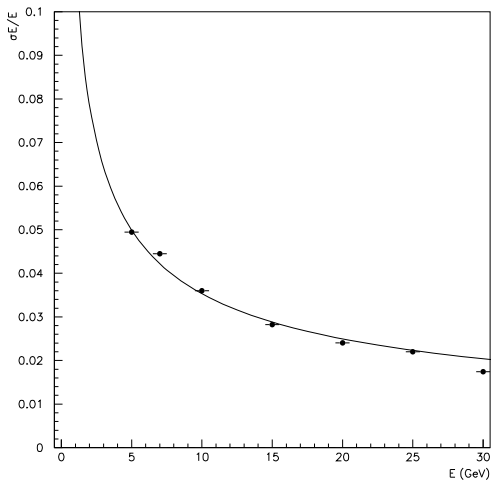

Figure 19: The energy resolution measured with a silicon-scintillator lead sandwich calorimeter.

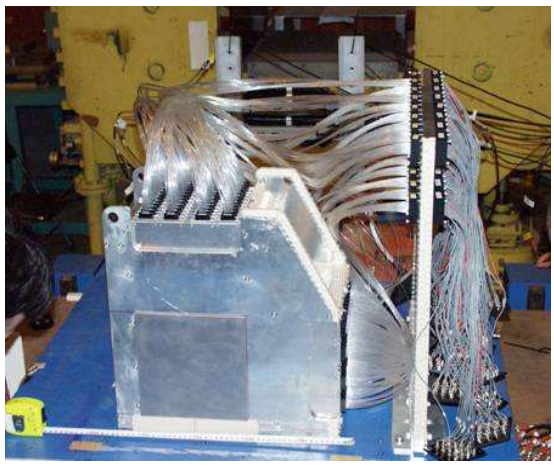

Figure 20: The prototype of a scintillator sandwich calorimeter measured in a test-beam. The size of the scintillator strips is 20x1x0.2 cm^3.

6.2. Hadron Calorimeters

Two technologies of sampling calorimeters are under investigation with either analog or digital readout. The analog read out calorimeter uses scintillator tiles as sensors. Digital calorimeters use GEMs or RPCs (Resistive Plate Chambers) as active elements.

6.2.1. Analog HCAL

The analog HCAL is designed with steel as absorber and scintillator tiles as sensors, each read out by a SiPM. A small prototype, the MINICAL, was operated successfully in a test-beam [29]. It was demonstrated that using SiPMs as photo-sensors maintains the resolution measured with classical photo-multipiers. Currently a 1 m^3 prototype calorimeter is being constructed by the CALICE Collaboration. The scintillator tiles in the core of the calorimeter are of 3x3 cm^2 size, each equipped with a SiPM. A full scintillator plane is shown in in Figure 21 [30]. The prototype will have 8000 analog channels. Readout electronics and DAQ are under development. The test of the first components was promising. The commissioning of the prototype will start soon in an electron beam. The test program in a hadron beam is foreseen for 2006.

6.2.2. Digital HCAL

The structure of a digital HCAL with GEMs as sensors [21] is shown in Figure 22. The size of the pads is 1x1 cm^2. Small test chambers are operated with cosmics and a radioactive source. Studies are done on the gas amplification for several gas mixtures. The efficiency, measured with cosmics, is found to be about 95%. In the fall of 2005 a 1 m^2 area module of GEM chambers will be tested and in 2006 a module of a digital HCAL will be ready for test-beam measurements [31].

In a different option RPCs are used as active detectors. Large area RPCs are tested and work very reliably [32]. The segmentation of the pick-up pads is the same as for the GEM option. The test of a fully equipped HCAL module is planned in 2007.

The medium term goal is a beam-test of a module consisting of prototypes of a silicon tungsten ECAL and prototypes of the different HCAL technologies pursued [33].

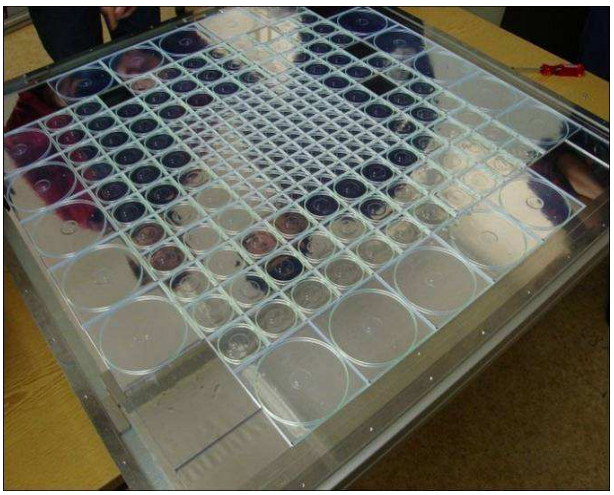

Figure 21: A scintillator tile plane for the 1 m^3 prototype calorimeter. Each tail is equipped with a wavelength shifting fiber read out by a SiPM.

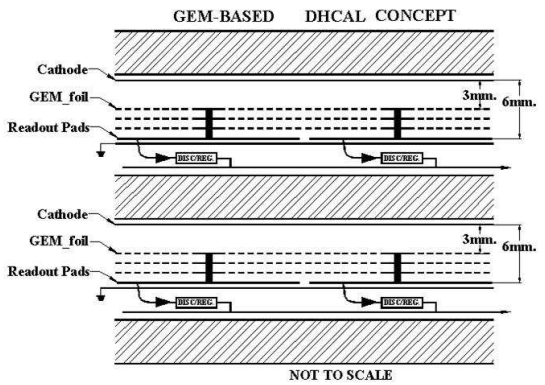

Figure 22: The structure of the digital HCAL equipped with GEMs. Gas amplification occurs in several GEM foils. The signal is picked up from cathode pads. The FE electronics unit is placed on the pad.

7. MUON DETECTION

The identification of muons is supported by detectors placed in the iron of the magnet return yoke. For the coverage of the large area RPCs or scintillator strips with fiber read out are considered. RPCs are characterised by a very good detection efficiency for mips and can cover large areas. Beam tests are done with several gas mixtures to optimise the working conditions. Long term tests are ongoing [34]. Large area scintillator planes are planned e.g. to be composed by extruded strips of 1m length, 10 cm width and 5mm thickness. A co-extruded hole along the strip is filled with a wavelength shifting fiber read out by a PM. Test done with a ^{90}Sr source have shown the high quality of the scintillator strips [35]. These strips will also be used for the 'tail catcher' in the joint ECAL-HCAL testbeam.

8. SUMMARY

A reach program of detector R&D is going on in all regions. The effort is focused on the design and development of prototypes of many sub-detectors, the mechanics design and the read out concepts. Several groups made already tests of prototype detectors in the beam. However, a lot of work is ahead to demonstrate that the benchmarks set by the challenging physics program are reached. Investigations of prototypes of all sub-detectors in test-beams must be performed. The results obtained in test-beam measurements are also needed to validate the simulations done to optimise the design of the detectors. For most of the sub-detectors several technologies are pursued. To make a fair comparison full system tests in the beam are mandatory. In this report I used results from many groups to demonstrate the status of the R&D. This is my personal choice, and it is not complete. I apologize to all the groups whose results I did not consider.

9. Acknowledgement

The following people helped me to prepare this talk: P. Checcia, Ch. Damerell, R. Fray, H. Kim, W. Lange, D. Peterson, A. Savoy-Navarro, R. Settles, Y. Sugimoto, M. Trimpl, N. Weerts, N. Wermes. Thank you.

References

[1] T. Behnke, *"Detector Concepts"*, to appear in the Proceedings of the ILCWS, Stanford, U.S.A. (2005).

[2] F. Richard, J.R. Schneider, D. Trines and A. Wagner, *"TESLA : Technical Design Report"*, DESY 2001-01, ECFA 2001-209, TESLA Report 2001-023, TESLA-FEL 2001-05 (2001).

[3] H. Abramowicz *et al.*, DESY PRC R&D 02/01 update 02(04), IEEE Trans. on Nucl. Science **51** (2004) 2983.

[4] C. Damerell, *"Vertex Detectors and the LC"*, to appear in the Proceedings of the ILCWS, Stanford, U.S.A. (2005).

[5] M. Breidenbach, http://www-conf.slac.stanford.edu/mdi/sessions/beamrf.htm.

[6] R. Kohrs *et al.*, DESY PRC R&D 03/01, Update 01(05).

[7] LCFI Collaboration, C. Damerell *et al.*, DESY PRC R&D 01/01, Update 02(05).

[8] G. Deptuch *et al.*, DESY PRC R&D 01/04, Update 02(05).

[9] The SLD Coll., Nucl. Instr. and Meth. **A400** (1997) 1898.

[10] Y. Sugimoto, *"Fine Pixel CCD Option for the ILC Vertex Detector"*, to appear in the Proceedings of the ILCWS, Stanford, U.S.A. (2005).

[11] D. Buskulic *et al.* Nucl. Instr. and Meth. **A360** (1995) 481.

[12] P. Abreu *et al.* Nucl. Instr. and Meth. **A378** (1996) 57.

[13] M. Killenberg *et al.*, DESY PRC R&D 01/03, Update 03(04),
D. Peterson *et al.*, http://www.hep.uiuc.edu/LCRD/LCRD_UCLC_proposal_FY05/.

[14] W. Chen *et al.*, DESY PRC R&D 03/02, Update 02(05).

[15] B. Schumm *et al.*, http://www.hep.uiuc.edu/LCRD/LCRD_UCLC_proposal_FY05/.

[16] J. Genat, *"Front-end Electronics for Large Silicon Trackers"*, to appear in the Proceedings of the ILCWS, Stanford, U.S.A. (2005).

[17] T. Nelson, *"Silicon Tracker Design for the ILC"*, to appear in the Proceedings of the ILCWS, Stanford, U.S.A. (2005).

[18] B. Cooper, *"Status of the SiD Silicon Tracker Mechanical Design"*, to appear in the Proceedings of the ILCWS, Stanford, U.S.A. (2005).

[19] K. Moenig, private communication.

[20] L. Sawyer *et al.*, http://www.hep.uiuc.edu/LCRD/LCRD_UCLC_proposal_FY05/.

[21] S. Valkar *et al.*, PRC R&D 01/02 update 01(04).

[22] G. Mavromanolakis, *"CALICE Si/W ECAL prototype, first testbeam results"*, to appear in the Proceedings of the ILCWS, Stanford, U.S.A. (2005).

[23] S. Nam, *"CERN Beam Test of Silicon-Tungsten Calorimeter Test Module"*, to appear in the Proceedings of the ILCWS, Stanford, U.S.A. (2005).

[24] Ch. De La Taille, *"VFE Future Developments"*, to appear in the Proceedings of the ILCWS, Stanford, U.S.A. (2005).

[25] D. Strom, *" First results with the prototype detectors of the Si/W ECAL"*, to appear in the Proceedings of the ILCWS, Stanford, U.S.A. (2005),
http://www.hep.uiuc.edu/LCRD/LCRD_UCLC_proposal_FY05/.

[26] M. Breidenbach, *"Design considerations for the Si/W ECAL electronics"*, to appear in the Proceedings of the ILCWS, Stanford, U.S.A. (2005).

[27] P. Checcia *et al.*, DESY PRC R&D 00/02 Update 01(03).

[28] A. Nagano, *"Study of strip electromagnetic calorimeter"*, Talk given at the ILC detector workshop, March 3-5 (2005), KEK, Japan.

[29] V. Andreev *et al.*, Nucl. Instr. and Meth. **A540** (2005) 368.

[30] F. Sefkow, *" Tile HCAL Testbeam Prototype"*, to appear in the Proceedings of the ILCWS, Stanford, U.S.A. (2005).

[31] A. White, *"Developments of GEMS"*, to appear in the Proceedings of the ILCWS, Stanford, U.S.A. (2005),

http://www.hep.uiuc.edu/LCRD/LCRD_UCLC_proposal_FY05/.

[32] J. Repond *"DHCAL prototype construction"*, to appear in the Proceedings of the ILCWS, Stanford, U.S.A. (2005),
http://www.hep.uiuc.edu/LCRD/LCRD_UCLC_proposal_FY05/.

[33] J. C. Brient and J. Yu, *"International Linear Collider Calorimeter/Muon Detector Test Beam Program"*, FNAL-TM-2291, 2005.

[34] M. Piccolo *" Glass RPC R&D Results"*, to appear in the Proceedings of the ILCWS, Stanford, U.S.A. (2005).

[35] A. Dychkant *" Studies of NICADD Extruded Scintillator Strips"*, to appear in the Proceedings of the ILCWS, Stanford, U.S.A. (2005).